

Dimethyl 2-Methylglutarate (Iris): A Green Platform for Efficient Liquid-Phase Exfoliation of 2D Materials


Gianluca D'Olimpio, Jessica Occhiuzzi, Luca Lozzi, Luca Ottaviano, and Antonio Politano*

Liquid-phase exfoliation of bulk crystals of layered materials, held together by weak interlayer van der Waals forces, is an ideal platform for scalable synthesis of nanosheets. However, it is mandatory to substitute existing solvents, regrettably displaying severe limitations due to toxicity. Here, dimethyl 2-methylglutarate (Rhodiasolv Iris) is validated for efficient liquid-phase exfoliation of selected van der Waals materials, namely, MoS₂, WS₂, GeSe, and graphite. Here, we show that Iris-assisted liquid phase exfoliation provides high yield (up to 52%) of flakes of 2D materials with aspect ratio as high as 500. Considering the various advantages of Iris over the state-of-the-art solvents, including the absence of toxicity and its biodegradability, this work opens new possibilities for the ecofriendly production of 2D materials and for their extensive usage in industrial processes hitherto semi-unexplored, owing to the toxicity of state-of-the-art solvents (including the production of drinkable water or fruit juice concentration). Accordingly, the validation of Iris for sustainable liquid-phase exfoliation of van der Waals crystals has intrinsic outstanding potential commercial impact. Moreover, here the values of the surface tension, Hansen solubility parameter, and viscosity of Rhodiasolv Iris are reported for the first time, which will be relevant also for any other sustainable process based on this new green solvent.

1. Introduction

The emergence of 2D materials^[1–8] had a tremendous impact on the scientific research, in consideration of the unique properties and their broad technological prospect in photonics,^[9] flexible electronics,^[10] nanocomposites,^[11,12] (photo)electrocatalysis,^[13–15] supercapacitors,^[16,17] functional coatings,^[18] (bio)sensors,^[19] and desalination.^[11,20–22]

G. D'Olimpio, J. Occhiuzzi, L. Lozzi, L. Ottaviano, A. Politano
Department of Physical and Chemical Sciences
University of L'Aquila
via Vetoio, L'Aquila 67100, Italy
E-mail: antonio.politano@univaq.it

 The ORCID identification number(s) for the author(s) of this article can be found under <https://doi.org/10.1002/adsu.202200277>.

© 2022 The Authors. Advanced Sustainable Systems published by Wiley-VCH GmbH. This is an open access article under the terms of the Creative Commons Attribution License, which permits use, distribution and reproduction in any medium, provided the original work is properly cited.

DOI: 10.1002/adsu.202200277

The large-scale manufacture of atomically thin layers is hitherto an important hurdle in the pathway for the industrial exploitation of 2D materials.^[23,24] While most basic investigations on 2D materials were performed on flakes prepared by mechanical exfoliation^[25] or on atomically thin layers synthesized by chemical vapor deposition,^[26] unfortunately such methods are unfeasible to tackle scalability. As a matter of fact, mechanical exfoliation is poorly reproducible and with scarce yield,^[25] while chemical vapor deposition is affected by the need of a suitable substrate,^[27] which should be successively etched and transferred,^[28] with the consequent insufficient crystallinity (owing to the unavoidable presence of defects^[29]) and cleanliness (associated to polymeric residuals in the successive transfer process^[30,31]) of produced 2D materials.

On the other hand, liquid-phase exfoliation (LPE) from parental bulk crystals is ideal for a scalable production of 2D materials, dispersed in solvents, suitable for their successive implementation.^[32] Solvents for LPE must minimize the energy cost for separating the sheets by breaking the weak interlayer van der Waals bonds. Specifically, the interfacial surface tension between the solid and the liquid should be minimized.^[33,34] Such models consider that the surface tension has two components: i) polar and ii) dispersive due to long-range interactions. By selecting the most opportune ratios between these quantities in the solvent and in the layered materials, the yield is maximized based on the minimization of the surface tension. Specifically^[33]

$$\begin{aligned}\sigma_{sl} &= \sigma_s + \sigma_l - 2\left(\sqrt{\sigma_s^d \cdot \sigma_l^d} + \sqrt{\sigma_s^p \cdot \sigma_l^p}\right) \\ &= \sigma_s^d + \sigma_s^p + \sigma_l^d + \sigma_l^p - 2\left(\sqrt{\sigma_s^d \cdot \sigma_l^d} + \sqrt{\sigma_s^p \cdot \sigma_l^p}\right)\end{aligned}\quad (1)$$

where σ_s is the surface tension of the solid (i.e., materials to be exfoliated) and σ_l is the surface tension of the liquid (i.e., the solvent). The superscripts “p” and “d” stand for polar and dispersive components, respectively. σ_{sl} is the interfacial surface tension between the material and the solvent, which should be minimized to optimize the efficiency of the exfoliation.

Table 1. Surface energy and Hansen solubility parameters of van der Waals crystals.

	Surface energy	Hansen solubility parameters		
	E_{sur} [mN m ⁻¹]	δ_d [MPa ^{1/2}]	δ_p [MPa ^{1/2}]	δ_H [MPa ^{1/2}]
WS ₂ ^[57]	≈75	16–18	5–14	2–19
MoS ₂ ^[57]	≈70	17–19	6–12	4.5–8.5
Graphite ^[52]	≈62	≈18	≈9.3	≈7.7
GeSe ^[58]	≈220	n.a.	n.a.	n.a.

Equation (1) can be also expressed as

$$\begin{aligned} \sigma_{s1} &= \left(\frac{\sigma_s^p}{\sigma_s^d} + 1 \right) \sigma_s^d + \left(\frac{\sigma_1^p}{\sigma_1^d} + 1 \right) \sigma_1^d - 2 \left(\sqrt{\frac{\sigma_1^p \sigma_s^p}{\sigma_1^d \sigma_s^d} + 1} \right) \sqrt{\sigma_1^d \sigma_s^p} \\ &= \left(\sqrt{\sigma_s^d} \sqrt{\frac{\sigma_s^p}{\sigma_s^d} + 1} - \sqrt{\sigma_1^d} \sqrt{\frac{\sigma_1^p}{\sigma_1^d} + 1} \right)^2 \\ &\quad + 2 \sqrt{\sigma_1^d \sigma_s^d} \left(\sqrt{\frac{\sigma_1^p}{\sigma_1^d} + 1} \sqrt{\frac{\sigma_s^p}{\sigma_s^d} + 1} - \sqrt{\frac{\sigma_1^p \sigma_s^p}{\sigma_1^d \sigma_s^d} - 1} \right) \end{aligned} \quad (2)$$

By inspecting Equation (2), it is evident that in order to minimize interfacial surface tension of 2D materials and solvents, the following conditions should be verified i) $\sigma_s^d \approx \sigma_1^d$ and ii) $\sigma_s^p \approx \sigma_1^p$ and, consequently,

$$\frac{\sigma_s^p}{\sigma_s^d} \approx \frac{\sigma_1^p}{\sigma_1^d} \quad (3)$$

Moreover, the dispersibility of nanosheets and solvent is another key issue, subject to the peculiar solvent-solute interaction, described by contemplating the Hansen solubility parameters (HSP) to account dispersion forces (δ_d), polar interactions (δ_p), and hydrogen bonds (δ_H).

Whensoever δ_d , δ_p , and δ_H are balanced for the solvent and the solute, the energy amount for their dispersion is minimized.

The most diffuse solvents for dispersion of van der Waals crystals are *N,N*-dimethylformamide (DMF) and NMP,^[35] owing to a good matching of their surface energy and HSP (reported in Table 1) with surface tension and HSP of solvents in Table 2.

Unfortunately, DMF and NMP show severe toxicity issues (including as reproductive toxin^[36]), which have determined restriction to their use in both USA^[37,38] and Europe (where they are listed among substances of very high concern^[39]).

Table 2. Surface tension and Hansen solubility parameters for Iris, NMP, DMF, IPA, and urea.

	Surface tension	Hansen solubility parameters		
	σ_s [mN m ⁻¹]	δ_d [MPa ^{1/2}]	δ_p [MPa ^{1/2}]	δ_H [MPa ^{1/2}]
Iris	33.0	16.6	8.7	5.0
NMP	40.1 ^[52]	18.0 ^[53]	12.3 ^[53]	7.2 ^[53]
DMF	37.1 ^[52]	17.4 ^[53]	13.7 ^[53]	11.3 ^[53]
IPA	21.7 ^[52]	15.8 ^[53]	6.1 ^[53]	16.4 ^[53]
Urea 30% in H ₂ O	74.0 ^[54]	17.0 ^[55]	16.7 ^[55]	38.0 ^[55]

Thus, the quest of an ecofriendly substitute to such standard aprotic solvents is mandatory. Several possible candidates show remarkable pitfall. As an example, volatile organic compounds (VOCs) display an insufficient exfoliation yield,^[40] with the need to transfer nanosheets from NMP suspensions.^[41] Moreover, most VOC exhibit flash temperatures as low as 10–13 °C, with consequent issues for safe industrial procedures.

Another possibility for LPE is represented by electrochemical exfoliation in electrolytes,^[37] which however requires the addition of conductive additives^[42] for insulating and semi-conducting samples. Moreover, it produces highly defective nanosheets^[37,43] with thickness far from the monolayer regime.^[44]

Moreover, for LPE assisted by urea aqueous solutions,^[45] the yield is as low as 2.4%, due to a surface tension significantly different from other solvents (Table 2).

On the other hand, residuals are unavoidable for LPE assisted by surfactants in aqueous media.^[46]

As regards dihydrolevoglucosenone (Cyrene), whose use in LPE has been recently explored,^[47] one should mention that its excessive dynamic viscosity (around 15 cP at room temperature) impedes any use in inkjet printing.

Manifestly, current methods using standard solvents inexorably inhibit the scalability of Flatland-based industry. Thus, the quest of a solvent enabling i) sustainable LPE and ii) high yield is mandatory.

Here, we validate the use of dimethyl 2-methylglutarate (Rhodiasolv Iris, CAS: 33514-22-6) as a polar solvent for sonication-assisted LPE of van der Waals crystals. Iris (C₈H₁₄O₄, Figure 1) does not display measurable toxicity for doses below 2000 mg kg⁻¹ d⁻¹. Its water solubility is higher than 25 g L⁻¹ at T = 23 °C. Notably, Iris has a flash point of 90.8 °C.^[48]

The sufficiently high dynamic viscosity (2.85 cP at T = 20 °C) enables suitable use in ink-jet printing of nanosheets-based devices, contrarily to NMP and DMF, which suffer poor jet performance, owing to a dynamic viscosity below 2 cP.^[49]

Specifically, by adopting as case-study examples MoS₂, WS₂, GeSe, and graphene, we demonstrate the suitability of Iris to produce atomically thin layers of layered materials by sonication-assisted LPE. The absence of any toxicity issues in Iris, with an exfoliation yield as high as 52%, enables the use of 2D materials in agri-food industry (including the production of potable water^[50] or fruit juices^[51]).

2. Results and Discussion

The value of the surface tension of Iris (33.0 mN m⁻¹, Table 2) resembles the cases of NMP and DMF, whereas it is lower by ≈35% in isopropyl alcohol (IPA).

By defining the surface tension (σ_s) as

$$\sigma_s = (E_{\text{Sur}} - TS_{\text{Sur}}) \quad (4)$$

where E_{Sur} corresponds to surface energy and S_{Sur} surface entropy and considering S_{Sur} for liquids generally is around 0.1 mN m⁻¹, one can conclude that generally a mismatch by at least 30 mN m⁻¹ exists between the surface energy of the van der Waals crystals with surface tensions of solvents at room temperature.^[56]

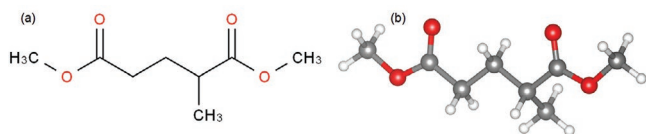


Figure 1. a) Plain and b) ball-and-stick representations of the atomic structure of dimethyl 2-methylglutarate (Iris).

The effectiveness of Iris to achieve high-yield dispersions of nanosheets was certified through an examination of dispersed flakes for selected cases of MoS₂, WS₂, GeSe, and graphite.

First, the yield of the process in terms of the amount of nanosheets with respect to the initial concentration was evaluated to range between 38% and 52% in all cases in the same conditions.

The inspection of atomic-resolution high-angle annular dark field-scanning transmission electron microscopy experiments (Figure 2b) of a MoS₂ flake identified in bright field (BF)-scanning transmission electron microscopy (STEM) (Figure 2a) corroborates the absence of structural damages in the basal plane of nanosheets. Accordingly, sonication-assisted LPE of van der Waals crystals with the Rhodiasolv Iris solvent just breaks weak interlayer van der Waals bonds. We were unable to detect defective regions, even for statistical analyses extended to 13 different samples.

Moreover, the lack of any modification in the electronic band structure was secured by UV-Vis absorption data (Figure 2c). Especially, observation of the peculiar absorptions at 674 and 612 nm related to the A and B excitons of MoS₂, originating

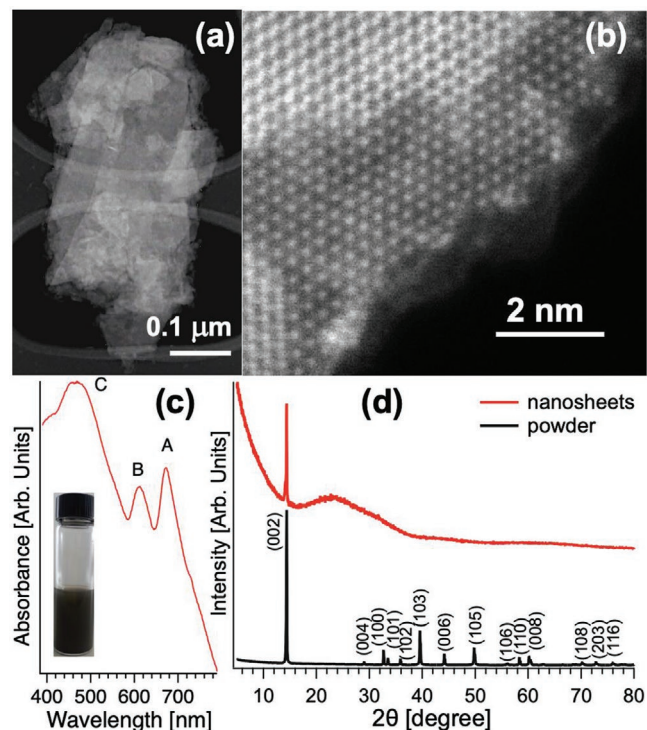


Figure 2. a) BF-STEM image with various nanosheets of MoS₂ on a lacey carbon grid. b) High-resolution high-angle annular dark field-STEM image for a self-standing nanosheet. c) UV-Vis spectrum of MoS₂ nanosheets produced by Iris-assisted LPE. d) XRD pattern of (black curve) powdered MoS₂ bulk crystals and (red curve) exfoliated nanosheets of MoS₂.

from the interband excitonic transition at the *K* point of the Brillouin zone,^[59–61] secures that the LPE in Iris solvent did not modify the electronic band structure of MoS₂.

The MoS₂ dispersion had a concentration of ≈0.18 mg mL⁻¹ (with a yield of ≈52% of the initial mass in the final dispersion). The stability of the dispersions was evaluated by acquiring daily photographs for 10 d, which indicated that 67% of the nanosheets persist in the dispersions after 10 d.

X-ray diffraction (XRD) measurements were used to evaluate the crystal structure of MoS₂ nanosheets obtained by Iris-assisted LPE with respect to the bulk MoS₂ (Figure 2d). Powders of bulk MoS₂ exhibited the characteristic XRD pattern of a hexagonal structure,^[62] with peaks matching with International Centre for Diffraction Data ref no. 04-003-3374. On the other hand, the appearance of a strong (002) reflection centered at 14.4° in the XRD pattern of exfoliated MoS₂ nanosheets secured their good crystallinity (Figure 2d), congruently with results in ref. [8].

Figure 3 shows the log-normal distribution of lateral size (peaked around ≈0.5 μm) and thickness (peaked around ≈6 nm) of MoS₂ nanosheets produced by Iris-assisted LPE, based on the statistical analysis of experiments by scanning electron microscope (SEM) and atomic force microscope (AFM).

To provide a straightforward comparative assessment of the exfoliation performances of Iris with respect to state-of-the-art solvents, in Section S1 in the Supporting Information, the results for the case of NMP-assisted LPE in the same processing conditions are reported. The statistical analyses on the thickness of exfoliated flakes revealed that a bimodal distribution with the second maximum located even at 30 nm, thus inferring an incomplete exfoliation of the parental bulk crystals, also clarified by supporting STEM images. Correspondingly, Iris-assisted LPE provides 98% of flakes with thickness below 15 nm.

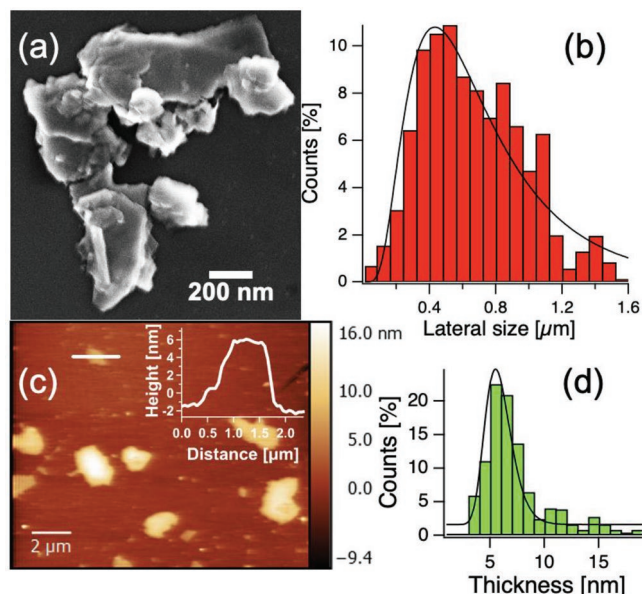


Figure 3. a) Selected high-resolution SEM picture of MoS₂ nanosheets. b) Distribution of lateral size of MoS₂ nanosheets based on SEM experiments. c) Selected AFM picture of MoS₂ flakes. The inset reports the height profile along the white solid line. d) Thickness distribution derived from AFM experiments.

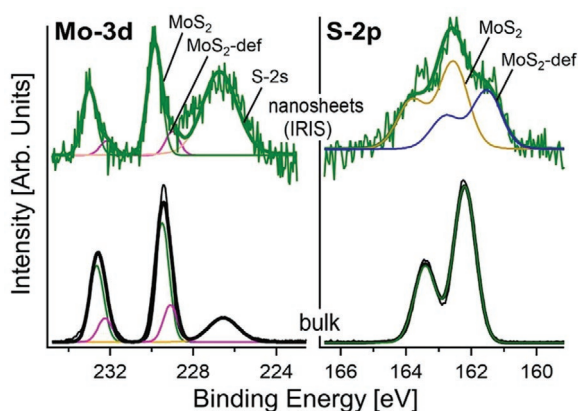


Figure 4. Mo-3d and S-2p core-level XPS spectra of bulk and nanosheets of MoS₂ exfoliated in Iris. The component at a BE of 226.7 eV in Mo-3d core level is related to the overlapping S-2s core level. The photon energy is 1486.6 eV (Al K_α) and the spectra are normalized to the maxima.

To assess eventual influence of LPE with Iris solvent on MoS₂, X-ray photoelectron spectroscopy (XPS) characterization was performed. Core-level spectra of bulk and exfoliated MoS₂ are shown in Figure 4. The Mo-3d core levels are split in $J = 5/2$ and $3/2$ components shifted by 3.1 eV. Specifically, XPS measurements indicate that Mo-3d core levels displays two different contributions arising from pristine (fully coordinated atoms)

and defective MoS₂ (sulfur vacancies, related to neighboring vacancy sites) with a binding energy (BE) of 229.8 and 229.0 eV for the $J = 5/2$ component, respectively, in agreement with previous works on MoS₂-based systems.^[63] Actually, defects introduce a minority component at lower BE, due to a redistribution of charge. Specifically, the charge localized on the more electronegative sulfur atom, once it is desorbed, is redistributed on the first neighboring atoms, so as to enhance the Coulomb screening effect.^[64–66] Notably, we note in Mo-3d spectra the absence of MoO₃-derived spectral features, which should appear at a BE of 232.4 eV for the $J = 5/2$ component.^[67] Therefore, we can conclude that Iris does not act as an oxidation agent for the MoS₂ nanosheets and, correspondingly, Iris-assisted liquid-phase exfoliation process does not favor the oxidation of MoS₂ flakes. Concerning the S-2p core levels, they are split in $J = 3/2$ and $1/2$ components shifted by 1.2 eV. Two well-distinct contributions associated to pristine and defective MoS₂ are observed at a BE of 162.5 and 161.5 eV for the $J = 3/2$ component, respectively, as in previous reports.^[64,65] Correspondingly, in S-2p core level no trace of sulfur-oxide phases was found.

To endorse the use of Iris as a suitable solvent for sonication-assisted LPE of van der Waals crystals, we validated its effectiveness for the cases of WS₂, graphite, and GeSe (Figure 5).

Panels (a–c) of Figure 5 report a representative SEM image of Iris-exfoliated WS₂, few-layer graphene, and GeSe nanosheets. Their corresponding distribution of lateral size and thickness are reported in panels (d–f) and (g–i), respectively.

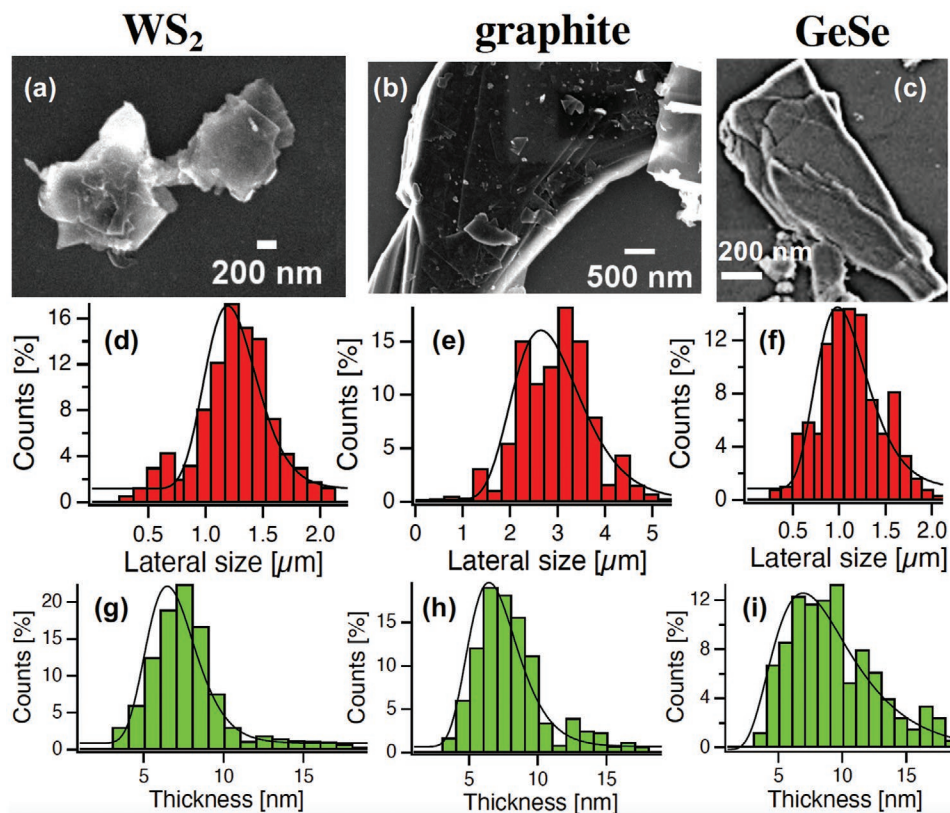


Figure 5. Selected SEM images of Iris-assisted LPE-exfoliated nanosheets of a) WS₂, b) graphite, and c) GeSe. Statistical analysis of d–f) lateral size and g–i) thickness of d,g) WS₂, e,h) graphite, and f,i) GeSe flakes, respectively.

As concerns WS₂ exfoliation, statistical analyses on both lateral size and thicknesses (Figure 5d,g) reveal similar values compared to the case of MoS₂. Precisely, the distribution of lateral size is centered around ≈1.2 μm, whereas the thickness distribution is peaked around 7 nm.

As regards the exfoliation of few-layer graphene flakes with Iris, the average lateral size exceeds 3 μm, with an average thickness of 7 nm.

GeSe flakes have average lateral area and thickness of 1 and 9 nm, respectively.

It is also important to remark that the use of other solvents for LPE of Ge bulk crystals could provide undesired effects. As an example, IPA provides nucleation of Se nanowires through abstraction of Se from the surface of GeSe flakes with the self-assembled formation of Se nanowires, as shown in SEM images in Section S2 in the Supporting Information.

Actually, for all case-study examples of van der Waals crystals studied for Iris, only 2D nanosheets with an aspect ratio exceeding 10² were obtained, with the highest aspect ratio being 500 for few-layer graphene.

It should be noticed that all types of the exfoliated 2D flakes have rugged edge (Figures 2, 3, and 5), while LPE assisted by other solvents, such as NMP, provides flakes with sharp edges with well-defined angle between, following some sort of crystallographic orientation (see Supporting Information, Figures S1–S3), congruently with findings in literature.^[68] Recently, Coleman and co-workers^[68] have demonstrated that, in the early stages of LPE, sonication induces the breakage of large flakes, with the formation of kink band striations on the flake surfaces, predominantly along zigzag directions. Then, cracking occurs along these striations and, together with intercalation of solvent, thin strips of van der Waals crystals are unzipped and peeled off, lastly affording atomically thin layers.

The above-mentioned difference regarding the shape of the flakes produced by Iris-assisted LPE could be rationalized by considering that, following suggestions by Bari et al.,^[69] the shape of edges and folds in nanosheets produced by sonication-assisted LPE are correlated to their bending moduli and sonication response. Correspondingly, the difference in the shape of the same crystal exfoliated with NMP and Iris could be correlated to the sonication response. One can infer that a key role could be played by the particularly reduced value of HSP of the Iris solvent, related to polar interactions (δ_p) and hydrogen bonds (δ_H), as reported in Table 2.

3. Conclusions

We have validated Iris as a suitable green solvent for producing atomically thin layers of van der Waals crystals with nanometric thickness and micrometric lateral size. Based on our results, one can propose that Iris could also substitute solvents usually used for all processes, such as shear mixing^[70] or wet-jet mill,^[71] particularly promising for industrial scale up. The efficiency of the Iris-based LPE process is crucial in order to combine intrinsic benefits for environmental health and safety with optimization of performances. Undeniably, the introduction of a green solvent for LPE also will expand the growing market of 2D materials toward fields to date nearly unexplored

(e.g., recovery of minerals from seawater, concentration of fruit juices, production of drinking water, etc.), as a result of the toxicity of state-of-the-art solvents for LPE, with subsequent superb impact on the commercial potential of their technological applications.

Moreover, here we have reported for the first time the values of the surface tension, Hansen solubility parameter, and viscosity of the new solvent Rhodiasolv Iris, remained unexplored so far. Such information will be relevant for sustainable processes based on this new green solvent.

4. Experimental Section

Materials: WS₂ (CAS Number 12138-09-9), MoS₂ (CAS Number 1317-33-5), and graphite (CAS Number 7782-42-5) were bought from Sigma-Aldrich. Dimethyl 2-methylglutarate (Rhodiasolv Iris) was provided by Rhodiasolv, Solvay Novocare, Paris.

Exfoliation of van der Waals Crystals: 0.04 g of powder of WS₂, MoS₂, and graphite were dispersed in 45 mL Rhodiasolv Iris and sonicated for 4 h in bath sonicator in a thermostat bath to avoid undesired temperature increase ($T \leq 24$ °C). To eliminate Iris, various centrifuges were performed. After a first centrifuge at 5000 rpm, supernatant was cast off and replaced with comparable quantity of ethanol. Then, a couple of further centrifuges were carried out to eliminate solvent residuals, with a final centrifuge at 1000 rpm to separate thinner flakes from thick and unexfoliated material. Conclusively, the supernatant was taken for spectroscopic and microscopic analyses.

Characterization: STEM investigation was performed with a JEOL ARM200F Cs-corrected microscope.

Field Emission Scanning Electron Microscope experiments were performed with Gemini SEM 500, at an accelerating voltage of 2 kV.

AFM measurements were performed with a Nanosurf NaioAFM instrument, using the Dynamic Force configuration with a dynamic mode cantilever. Used tips had a spring constant of 48 N m⁻¹ and resonance frequency of 190 kHz.

UV–vis absorption was measured with spectrometer by Perkin Elmer (Lambda 750).

XPS measurements were carried out with a PHI 1257 spectrometer with a monochromatic Al K_α source ($h\nu = 1486.6$ eV). The experimental resolution was 0.3 eV.

XRD experiments were performed at Instituto de Ciencia de Materiales de Barcelona of Consejo Superior de Investigaciones Científicas (CSIC) (ICMAB-CSIC), Barcelona, Spain using a point detector in θ - 2θ configuration using a Bruker-AXS (model A25 D8 Discover).

Supporting Information

Supporting Information is available from the Wiley Online Library or from the author.

Acknowledgements

G.D. and J.O. contributed equally to this work. A.P. acknowledges Solvay for having provided Rhodiasolv Iris. This research was conducted within the framework of an Innovative Industrial PhD project by J.O. under the supervision of A.P., supported by the PON Ricerca e Innovazione 2014/20. Francesc Xavier Campos is acknowledged for his support on XRD characterization. This project has received funding from the EU-H2020 research and innovation program under Grant Agreement 654360, Nanoscience Foundries and Fine Analysis (NFFA)-Europe through the access at Instituto de Ciencia de Materiales de Barcelona of CSIC (ICMAB-CSIC), Barcelona, Spain.

Open access funding provided by Universita degli Studi dell'Aquila within the CRUI-CARE Agreement.

Conflict of Interest

The authors declare no conflict of interest.

Data Availability Statement

The data that support the findings of this study are available from the corresponding author upon reasonable request.

Keywords

2D materials, green chemistry, Iris, liquid-phase exfoliations

Received: June 19, 2022

Revised: July 26, 2022

Published online:

- [1] X. Ren, Y. Tian, F. Shaik, J. Yang, R. Liu, K. Guo, B. Jiang, *Adv. Sustainable Syst.* **2022**, 6, 2100436.
- [2] A. Anouar, R. Garcia-Aboal, P. Atienzar, A. Franconetti, N. Katir, A. El Kadib, A. Primo, H. Garcia, *Adv. Sustainable Syst.* **2022**, 6, 2100487.
- [3] K. Sathiyar, A. Lal, A. Borenstein, *Adv. Sustainable Syst.* **2022**, 6, 2200076.
- [4] J. S. Arya Nair, S. Saisree, K. Y. Sandhya, *Adv. Sustainable Syst.* **2022**, 2200039.
- [5] M. Y. Yu, C. Li, W. Li, P. Min, *Adv. Sustainable Syst.* **2022**, 6, 2200023.
- [6] M. Reina, A. Scalia, G. Auxilia, M. Fontana, F. Bella, S. Ferrero, A. Lamberti, *Adv. Sustainable Syst.* **2022**, 6, 2100228.
- [7] Y. Wang, L. Wang, X. Zhang, X. Liang, Y. Feng, W. Feng, *Nano Today* **2021**, 37, 101059.
- [8] D. Gopalakrishnan, D. Damien, M. M. Shaijumon, *ACS Nano* **2014**, 8, 5297.
- [9] C. Lee, S. Kim, Y. H. Cho, *Adv. Sustainable Syst.* **2022**, 6, 2000216.
- [10] D. Jiang, Z. Liu, Z. Xiao, Z. Qian, Y. Sun, Z. Zeng, R. Wang, *J. Mater. Chem. A* **2022**, 10, 89.
- [11] N. Li, J. Ma, Y. Zhang, L. Zhang, T. Jiao, *Adv. Sustainable Syst.* **2022**, 6, 2200106.
- [12] Q. Dai, Z. Liu, L. Huang, C. Wang, Y. Zhao, Q. Fu, A. Zheng, H. Zhang, X. Li, *Nat. Commun.* **2020**, 11, 13.
- [13] Z. Xiao, X. Gan, T. Zhu, D. Lei, H. Zhao, P. Wang, *Adv. Sustainable Syst.* **2022**, 6, 2100515.
- [14] X. Pang, S. Xue, T. Zhou, M. Qiao, H. Li, X. Liu, Q. Xu, G. Liu, W. Lei, *Adv. Sustainable Syst.* **2022**, 2100507.
- [15] Y. Wang, F. Zhao, Y. Wang, Y. Zhang, Y. Shen, Y. Feng, W. Feng, *Compos. Commun.* **2022**, 32, 101175.
- [16] Z. Bai, D. Zhang, Y. Guo, Y. Yang, H. Yan, Y. Wang, J. Cheng, P. K. Chu, H. Pang, Y. Luo, *Adv. Sustainable Syst.* **2022**, 6, 2100371.
- [17] Y. Xu, M. Peng, K. Zhang, L. Wang, J. Chen, T. Hu, K. Yuan, *Adv. Sustainable Syst.* **2022**, 6, 2100414.
- [18] W. Han, Z. Wu, Y. Li, Y. Wang, *Chem. Eng. J. (Lausanne)* **2019**, 358, 1022.
- [19] V. Galstyan, A. Moumen, G. W. C. Kumaraage, E. Comini, *Sens. Actuators, B* **2022**, 357, 131466.
- [20] S. Xiao, X. Zhao, S. Liu, Y. Xue, G. Li, J. Yang, *Adv. Sustainable Syst.* **2022**, 6, 2100500.
- [21] R. Zha, T. Shi, L. He, M. Zhang, *Adv. Sustainable Syst.* **2022**, 6, 2100302.
- [22] E. Baigorria, L. F. Fraceto, *Adv. Sustainable Syst.* **2022**, 6, 2100243.
- [23] N. Kumar, R. Salehiyan, V. Chauke, O. J. Botlhoko, K. Setshedi, M. Scriba, M. Masukume, S. S. Ray, *FlatChem* **2021**, 27, 100224.
- [24] A. Zavabeti, A. Jannat, L. Zhong, A. A. Haidry, Z. Yao, J. Z. Ou, *Nano-Micro Lett.* **2020**, 12, 66.
- [25] L. Ottaviano, S. Palleschi, F. Perrozzi, G. D'Olimpio, F. Priante, M. Donarelli, P. Benassi, M. Nardone, M. Gonchigsuren, M. Gombosuren, A. Lucia, G. Moccia, O. A. Cacioppo, *2D Mater.* **2017**, 4, 045013.
- [26] K. Chen, L. Shi, Y. Zhang, Z. Liu, *Chem. Soc. Rev.* **2018**, 47, 3018.
- [27] Q. Ji, Y. Zhang, Y. Zhang, Z. Liu, *Chem. Soc. Rev.* **2015**, 44, 2587.
- [28] J. Qu, B.-W. Li, Y. Shen, S. Huo, Y. Xu, S. Liu, B. Song, H. Wang, C. Hu, W. Feng, *ACS Appl. Mater. Interfaces* **2019**, 11, 16272.
- [29] S. Wang, A. Robertson, J. H. Warner, *Chem. Soc. Rev.* **2018**, 47, 6764.
- [30] M. Chen, R. C. Haddon, R. Yan, E. Bekyarova, *Mater. Horiz.* **2017**, 4, 1054.
- [31] X. Yang, M. Yan, *Nano Res.* **2020**, 13, 599.
- [32] X. Zheng, H. Cong, T. Yang, K. Ji, C. Wang, M. Chen, *Nanotechnology* **2022**, 33, 185602.
- [33] J. Shen, Y. He, J. Wu, C. Gao, K. Keyshar, X. Zhang, Y. Yang, M. Ye, R. Vajtai, J. Lou, *Nano Lett.* **2015**, 15, 5449.
- [34] M. Wang, X. Xu, Y. Ge, P. Dong, R. Baines, P. M. Ajayan, M. Ye, J. Shen, *ACS Appl. Mater. Interfaces* **2017**, 9, 9168.
- [35] Y. Xu, H. Cao, Y. Xue, B. Li, W. Cai, *Nanomaterials* **2018**, 8, 942.
- [36] K. Sitarek, J. Stetkiewicz, *Int. J. Occup. Environ. Health* **2008**, 21, 73.
- [37] Y. Yang, H. Hou, G. Zou, W. Shi, H. Shuai, J. Li, X. Ji, *Nanoscale* **2019**, 11, 16.
- [38] A. Llevot, E. Grau, S. Carlotti, S. Grelier, H. Cramail, *Eur. Polym. J.* **2015**, 67, 409.
- [39] F. Bozso, P. Avouris, *Chem. Phys. Lett.* **1986**, 125, 531.
- [40] A. O'Neill, U. Khan, P. N. Nirmalraj, J. Boland, J. N. Coleman, *J. Phys. Chem. C* **2011**, 115, 5422.
- [41] X. Zhang, A. C. Coleman, N. Katsonis, W. R. Browne, B. J. Van Wees, B. L. Feringa, *Chem. Commun.* **2010**, 46, 7539.
- [42] F. Li, M. Xue, X. Zhang, L. Chen, G. P. Knowles, D. R. MacFarlane, J. Zhang, *Adv. Energy Mater.* **2018**, 8, 1702794.
- [43] Z. Y. Xia, S. Pezzini, E. Treossi, G. Giambastiani, F. Corticelli, V. Morandi, A. Zanelli, V. Bellani, V. Palermo, *Adv. Funct. Mater.* **2013**, 23, 4756.
- [44] Z. Zeng, Z. Yin, X. Huang, H. Li, Q. He, G. Lu, F. Boey, H. Zhang, *Angew. Chem.* **2011**, 50, 11093.
- [45] P. He, C. Zhou, S. Tian, J. Sun, S. Yang, G. Ding, X. Xie, M. Jiang, *Chem. Commun.* **2015**, 51, 4651.
- [46] M. Lotya, Y. Hernandez, P. J. King, R. J. Smith, V. Nicolosi, L. S. Karlsson, F. M. Blighe, S. De, Z. Wang, I. McGovern, *J. Am. Chem. Soc.* **2009**, 131, 3611.
- [47] H. J. Salavagione, J. Sherwood, V. Budarin, G. Ellis, J. Clark, P. Shuttleworth, *Green Chem.* **2017**, 19, 2550.
- [48] <https://echa.europa.eu/de/regISTRATION-dossier/-/registered-dossier/2181/9>.
- [49] J. Li, M. C. Lemme, M. Östling, *ChemPhysChem* **2014**, 15, 3427.
- [50] A. Gugliuzza, A. Politano, E. Drioli, *Curr. Opin. Chem. Eng.* **2017**, 16, 78.
- [51] G. D. Arend, K. Rezzadori, L. S. Soares, J. C. C. Petrus, *J. Food Sci. Technol.* **2019**, 56, 2312.
- [52] Y. Hernandez, V. Nicolosi, M. Lotya, F. M. Blighe, Z. Sun, S. De, I. T. McGovern, B. Holland, M. Byrne, Y. K. Gun'ko, J. J. Boland, P. Niraj, G. Duesberg, S. Krishnamurthy, R. Goodhue, J. Hutchison, V. Scardaci, A. C. Ferrari, J. N. Coleman, *Nat. Nanotechnol.* **2008**, 3, 563.
- [53] Y. Hernandez, M. Lotya, D. Rickard, S. D. Bergin, J. N. Coleman, *Langmuir* **2009**, 26, 3208.

- [54] S. Halonen, T. Kangas, M. Haataja, U. Lassi, *Emiss. Control Sci. Technol.* **2017**, 3, 161.
- [55] A. Aghanouri, G. Sun, *ACS Sustainable Chem. Eng.* **2016**, 4, 2337.
- [56] J. Lyklema, *Colloids Surf., A* **1999**, 156, 413.
- [57] J. N. Coleman, M. Lotya, A. O'Neill, S. D. Bergin, P. J. King, U. Khan, K. Young, A. Gaucher, S. De, R. J. Smith, I. V. Shvets, S. K. Arora, G. Stanton, H.-Y. Kim, K. Lee, G. T. Kim, G. S. Duesberg, T. Hallam, J. J. Boland, J. J. Wang, J. F. Donegan, J. C. Grunlan, G. Moriarty, A. Shmeliov, R. J. Nicholls, J. M. Perkins, E. M. Grieveson, K. Theuvsissen, D. W. McComb, P. D. Nellist, *Science* **2011**, 331, 568.
- [58] G. Bianca, M. I. Zappia, S. Bellani, Z. k. Sofer, M. Serri, L. Najafi, R. Oropesa-Nuñez, B. Martín-García, T. s. Hartman, L. Leoncino, *ACS Appl. Mater. Interfaces* **2020**, 12, 48598.
- [59] A. Splendiani, L. Sun, Y. Zhang, T. Li, J. Kim, C. Y. Chim, G. Galli, F. Wang, *Nano Lett.* **2010**, 10, 1271.
- [60] K. F. Mak, C. Lee, J. Hone, J. Shan, T. F. Heinz, *Phys. Rev. Lett.* **2010**, 105, 136805.
- [61] K. Wang, Y. Feng, C. Chang, J. Zhan, C. Wang, Q. Zhao, J. N. Coleman, L. Zhang, W. J. Blau, J. Wang, *Nanoscale* **2014**, 6, 10530.
- [62] P. Joensen, E. Crozier, N. Alberding, R. Frindt, *J. Phys. C* **1987**, 20, 4043.
- [63] M. Donarelli, F. Bisti, F. Perrozzi, L. Ottaviano, *Chem. Phys. Lett.* **2013**, 588, 198.
- [64] A. Di Paola, L. Palmisano, A. Venezia, V. Augugliaro, *J. Phys. Chem. B* **1999**, 103, 8236.
- [65] K. Wong, X. Lu, J. Cotter, D. Eadie, P. Wong, K. Mitchell, *Wear* **2008**, 264, 526.
- [66] A. Shpak, A. Korduban, L. Kulikov, T. Kryshchuk, N. Konig, V. Kandyba, *J. Electron Spectrosc. Relat. Phenom.* **2010**, 181, 234.
- [67] N. V. Alov, *Phys. Status Solidi C* **2015**, 12, 263.
- [68] Z. Li, R. J. Young, C. Backes, W. Zhao, X. Zhang, A. A. Zhukov, E. Tillotson, A. P. Conlan, F. Ding, S. J. Haigh, K. S. Novoselov, J. N. Coleman, *ACS Nano* **2020**, 14, 10976.
- [69] R. Bari, D. Parviz, F. Khabaz, C. D. Klaassen, S. D. Metzler, M. J. Hansen, R. Khare, M. J. Green, *Phys. Chem. Chem. Phys.* **2015**, 17, 9383.
- [70] S. Bicca, S. Barwich, D. Boland, A. Harvey, D. Hanlon, N. McEvoy, J. N. Coleman, *2D Mater.* **2018**, 6, 015008.
- [71] Y. Tominaga, K. Sato, D. Shimamoto, Y. Imai, Y. Hotta, *Ceram. Int.* **2015**, 41, 10512.